Supplementary Figures and Legends

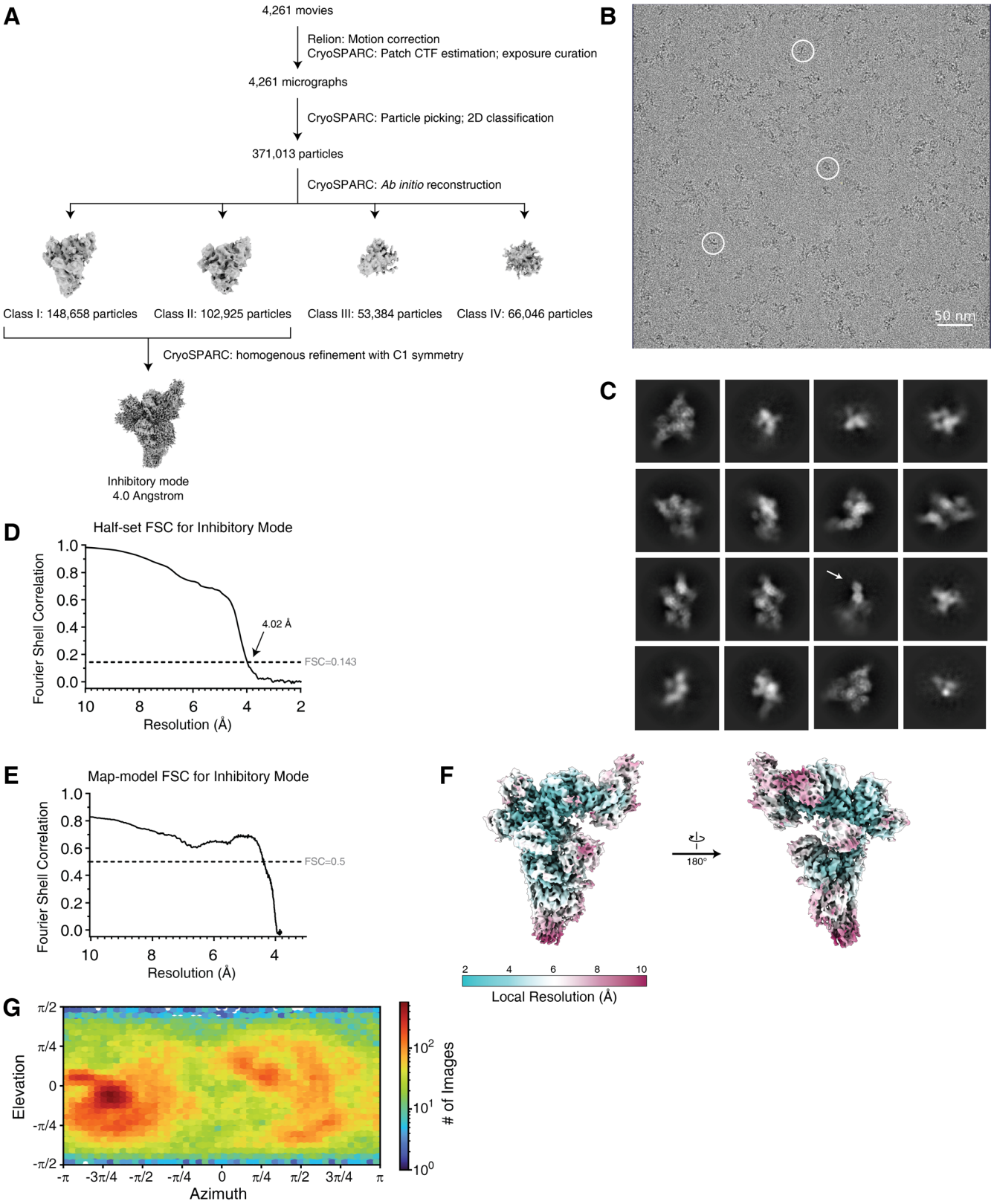

Figure S1. Structural determination of the GATOR1-Rag-Ragulator complex in the inhibitory mode (Related to Figure 3).

A. Workflow for the data processing of the GATOR1-Rag-Ragulator Inhibitory mode complex.

B. A sample raw cryo-EM image for this dataset. Exemplary particles used for data processing shown in white circles.
C. 2D clustering of extracted particles. Clustering reveals recognizable features, including the Rag-Ragulator extension pointing away from the GATOR1 complex (arrow).
D. Half-set gold-standard Fourier shell correlation (FCS) for the Inhibitory mode complex.
E. Map-model FSC for the Inhibitory mode complex.
F. Local resolution estimation of the GATOR1-Rag-Ragulator cryo-EM density map.
G. Orientation distribution plot for the Inhibitory mode complex.

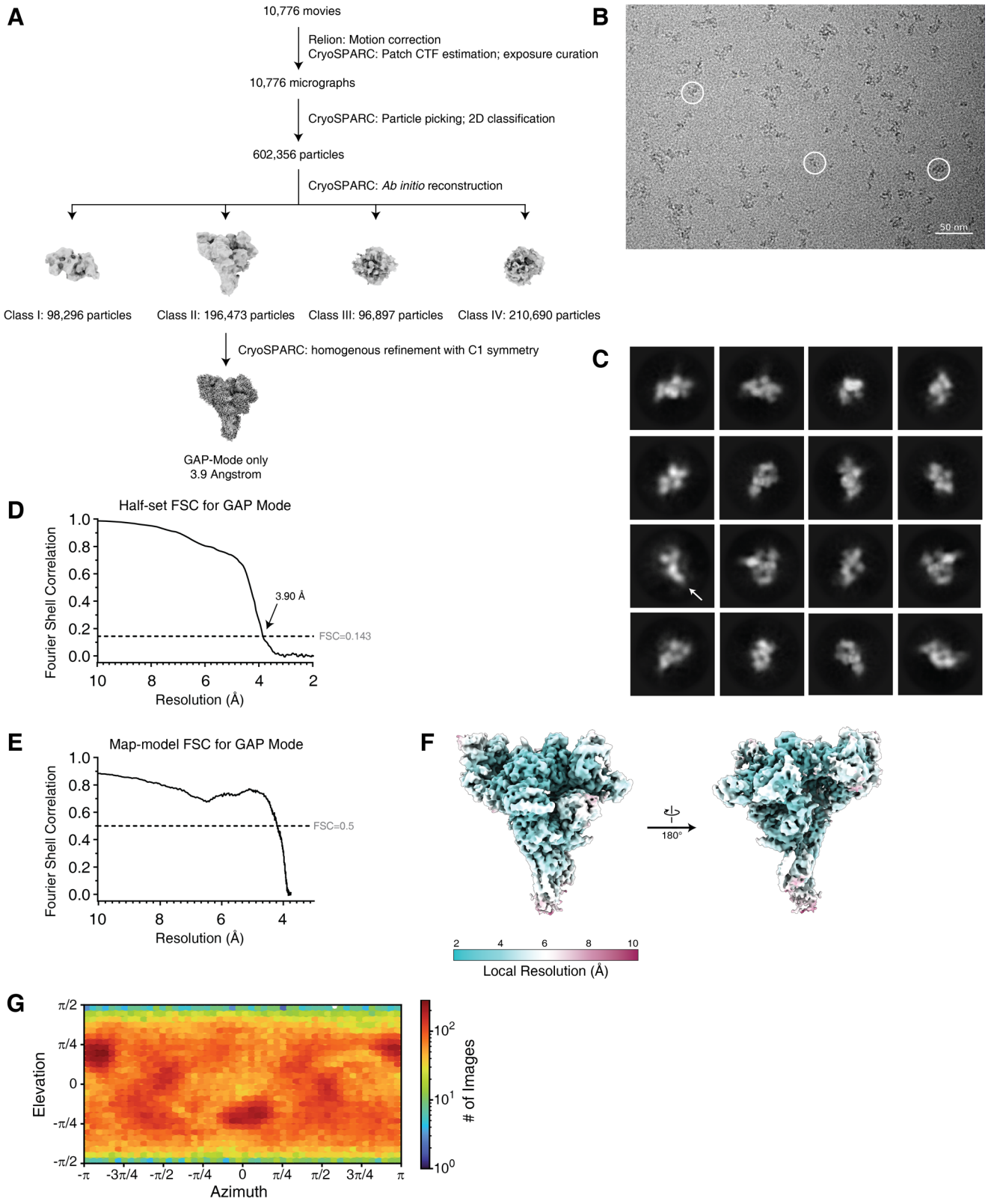

Figure S2. Structural determination of the GATOR1-Rag-Ragulator complex in the GAP mode (Related to Figure 3).

A. Workflow for the data processing of the GATOR1-Rag-Ragulator GAP mode complex.
B. A sample raw cryo-EM image for this dataset. Exemplary particles used for data processing shown in white circles.
C. 2D clustering of extracted particles. Clustering reveals distinguishable features (arrow).
D. Half-set gold-standard Fourier shell correlation (FCS) for the GAP mode complex.

E. Map-model FSC for the GAP mode complex.
F. Local resolution estimation of the GATOR1-Rag-Ragulator cryo-EM density map.
G. Orientation distribution plot for the GAP mode complex.

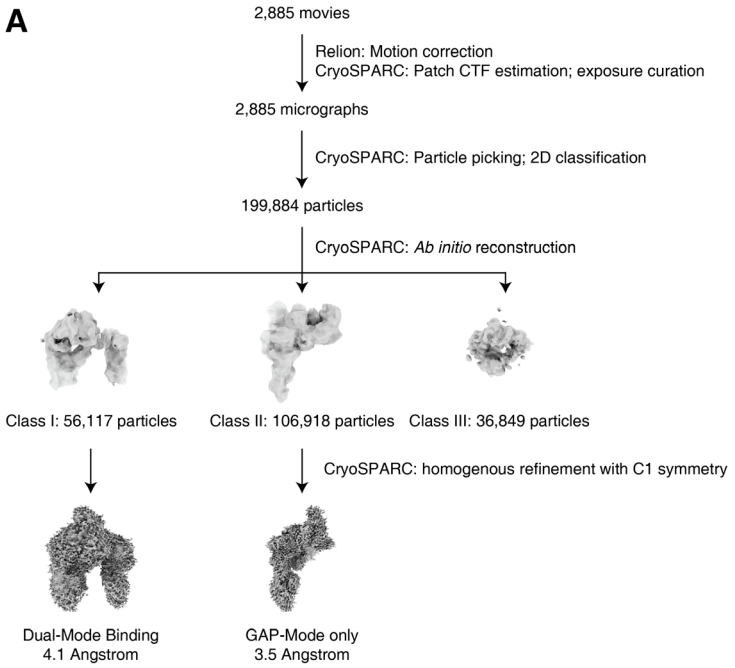
A
2,885 movies
Relion: Motion correction
CryoSPARC: Patch CTF estimation; exposure curation
2,885 micrographs
CryoSPARC: Particle picking; 2D classification
199,884 particles
CryoSPARC: Ab initio reconstruction
Class I: 56,117 particles
Class II: 106,918 particles
Class III: 36,849 particles
CryoSPARC: homogenous refinement with C1 symmetry
Dual-Mode Binding
4.1 Angstrom
GAP-Mode only
3.5 Angstrom


B
50 nm

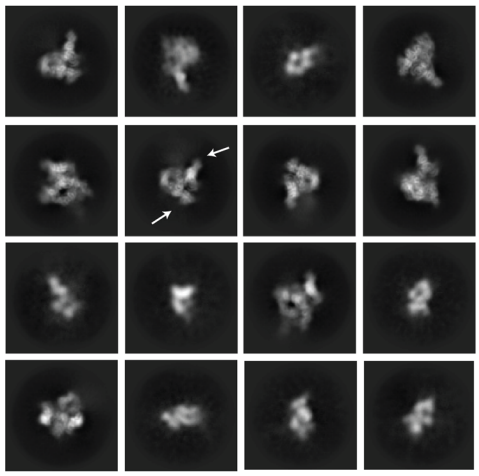
C

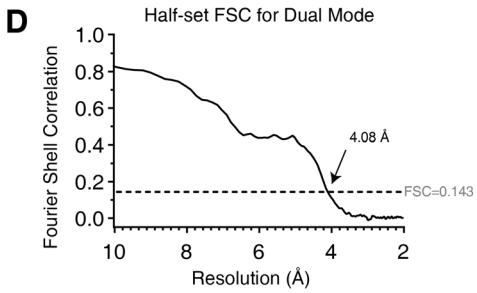
D
Half-set FSC for Dual Mode
Fourier Shell Correlation
Resolution (Å)
4.08 Å
FSC=0.143

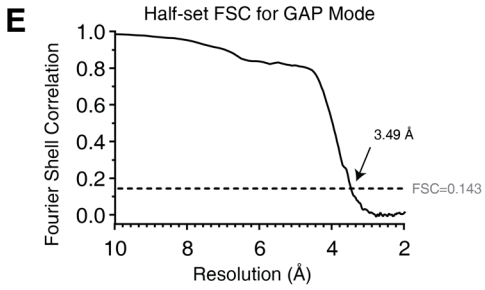
E
Half-set FSC for GAP Mode
Fourier Shell Correlation
Resolution (Å)
3.49 Å
FSC=0.143

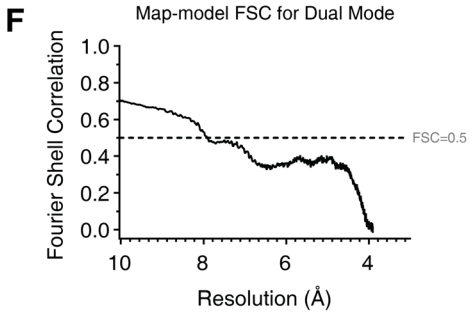
F
Map-model FSC for Dual Mode
Fourier Shell Correlation
Resolution (Å)
FSC=0.5

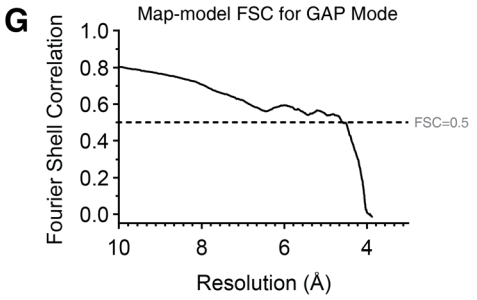
G
Map-model FSC for GAP Mode
Fourier Shell Correlation
Resolution (Å)
FSC=0.5

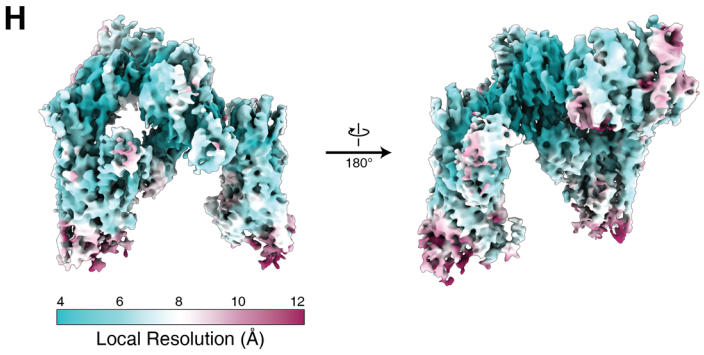
H
180°
Local Resolution (Å)

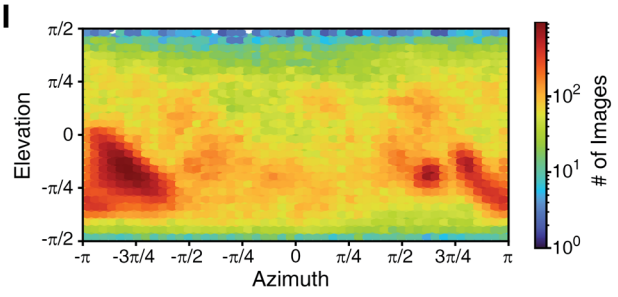
I
Elevation
Azimuth
# of Images

Figure S3. Structural determination of the GATOR1-Rag-Ragulator complex in the dual mode (Related to Figure 3).

A. Workflow for the data processing of the GATOR1-Rag-Ragulator Dual mode complex.
B. A sample raw cryo-EM image for this dataset. Exemplary particles used for data processing shown in white circles.
C. 2D clustering of extracted particles. Clustering reveals distinguishable features (arrow).
D. Half-set gold-standard Fourier shell correlation (FCS) for the Dual mode complex.
E. Half-set gold-standard Fourier shell correlation (FCS) for the GAP mode complex.
F. Map-model FSC for the dual mode complex.
G. Map-model FSC for the GAP mode complex.
H. Local resolution estimation of the GATOR1-Rag-Ragulator cryo-EM density map.
I. Orientation distribution plot for the Dual mode complex.

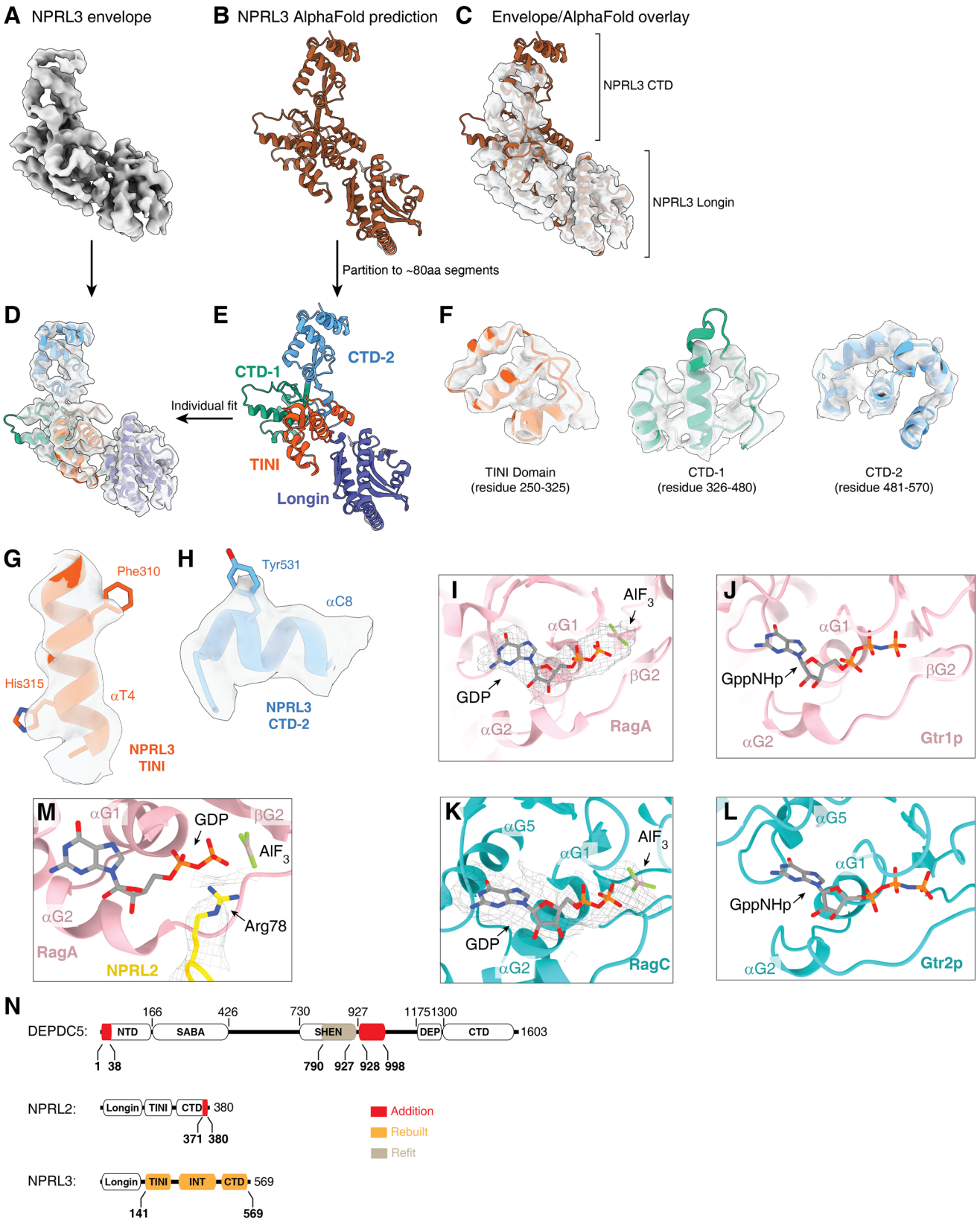

Figure S4. Model building and refinement (Related to Figure 3).

A. NPRL3 cryo-EM density map from the GATOR1-Rag-Ragulator GAP mode dataset.
B. NPRL3 structural model from AlphaFold (AF) prediction.
C. Direct overlay of density map and AF prediction.
D. Overlay of individual NPRL3 domains predicted from AF.
E. Partitioned domains from AF prediction algorithm.
F. Individual domains (i.e. TINI, CTD-1, CTD-2) overlaid with cryo-EM density map.

G. Bulky residues located on αT4 of the NPRL3 TINI domain used to ensure the amino acid register was fit properly.
H. Bulky residues located on αC8 of the NPRL3 CTD-2 domain used to ensure the amino acid register was fit properly.
I. Extra electron density within the nucleotide binding pocket of RagA corresponds to bound nucleotide, GDP:AlF_3, in the GAP mode structure.
J. Crystal structure of the GppNHp-bound RagA analog, Gtr1p, nucleotide binding pocket (PDB: 3R7W).
K. Extra electron density within the nucleotide binding pocket of RagC corresponds to bound nucleotide, GDP:AlF_3, in the GAP mode structure.
L. Crystal structure of the GppNHp-bound RagA analog, Gtr2p, nucleotide binding pocket (PDB: 3R7W).
M. Electron density of Arg-78 of NPRL2 in the GAP mode structure.
N. Comparison between the original GATOR1 model (PDB: 6CET) and updated GATOR1 model.

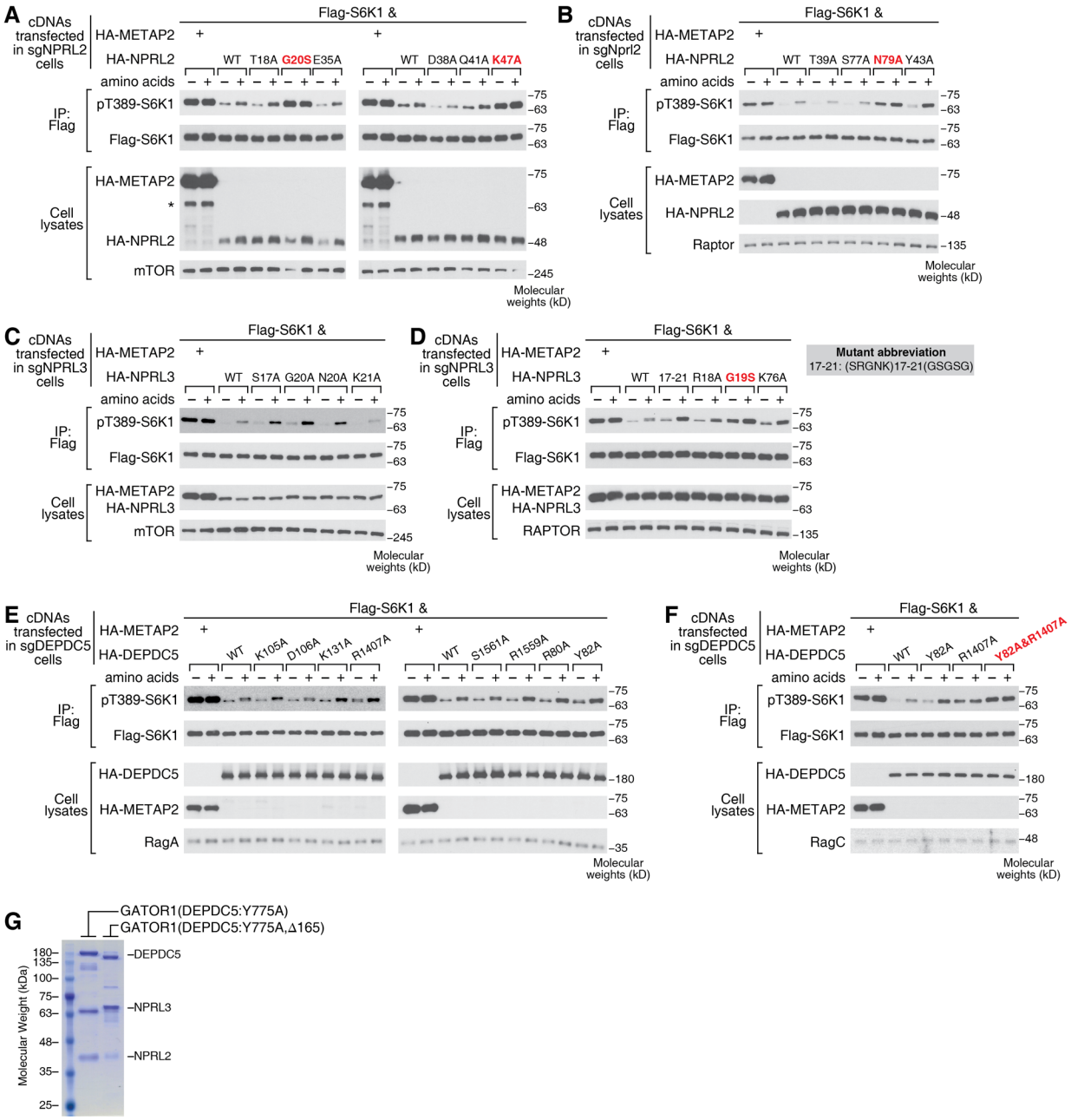

Figure S5. Effect of GATOR1 mutations on mTORC1 signaling in response to amino acids in cells (Related to Figure 4 and Figure 5).

A & B. Effect of expression of various NPRL2 mutants in sgNPRL2 cells on the ability to restore mTORC1 signalling in the presence and absence of amino acids.

C & D. Effect of expression of various NPRL3 mutants in sgNPRL3 cells on the ability to restore mTORC1 signalling in the presence and absence of amino acids.

E & F. Effect of expression of various DEPDC5 mutants in sgDEPDC5 cells on the ability to restore mTORC1 signalling in the presence and absence of amino acids.

G. Coomassie staining gel of recombinantly expressed and purified GATOR1[DEPDC5(Y775A)] and GATOR1[DEPDC5(Δ165, Y775A)] protein complexes.

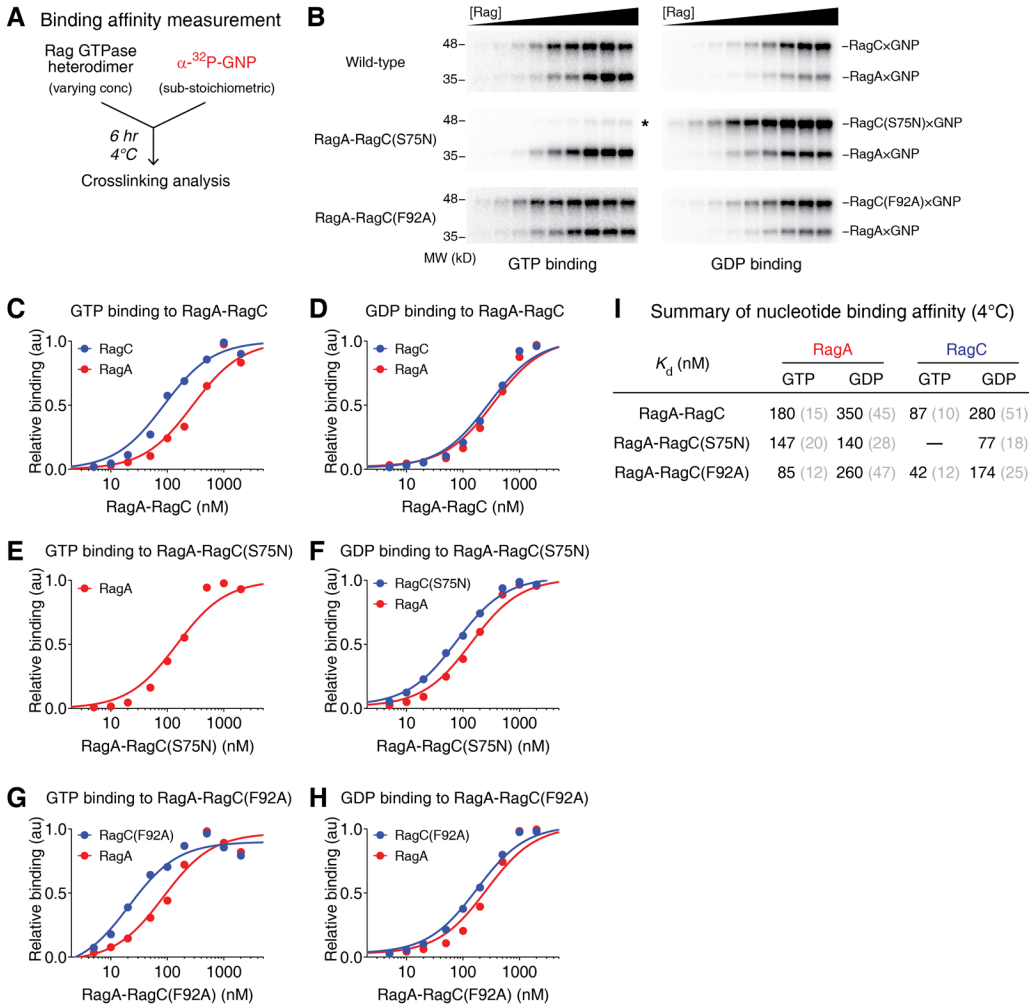

I Summary of nucleotide binding affinity (4°C)

K_d (nM)	RagA		RagC	
	GTP	GDP	GTP	GDP
RagA-RagC	180 (15)	350 (45)	87 (10)	280 (51)
RagA-RagC(S75N)	147 (20)	140 (28)	—	77 (18)
RagA-RagC(F92A)	85 (12)	260 (47)	42 (12)	174 (25)

Figure S6. Nucleotide binding properties of RagA-RagC and mutants (Related to Figure 6).

A. Equilibrium binding assay to assess GTP and GDP affinity towards individual Rag subunit.

B. SDS-PAGE gel to assess nucleotide binding to Rag GTPases. GTP binding (left) and GDP binding (right) measure the dissociation constants (K_d) of nucleotides. Asterisk indicates an inability to determine GTP binding to the RagA-RagC(S75N) mutant due to the known disruption of binding that this mutation induces.

C & D. Quantification of the radioactive signals from panel B for the wild-type RagA-RagC binding to GTP (C), or GDP (D). A single-site binding equation was fit to determine the dissociation constant of both nucleotides K_d. This experiment was repeated three times and a representative was shown here. A.U., arbitrary units.

E & F. Quantification of the radioactive signals from panel B for the mutant RagA-RagC(S75N) binding to GTP (C), or GDP (D). A single-site binding equation was fit to determine the dissociation constant of both nucleotides K_d. This experiment was repeated three times and a representative was shown here. A.U., arbitrary units.

G & H. Quantification of the radioactive signals from panel B for the mutant RagA-RagC(F92A) binding to GTP (C), or GDP (D). A single-site binding equation was fit to determine the dissociation constant of both nucleotides K_d. This experiment was repeated three times and a representative was shown here. A.U., arbitrary units.

I. Summary of the dissociation constants (K_d) of nucleotides at 4 °C. Experiments were performed three times, and the mean ± SEM reported.

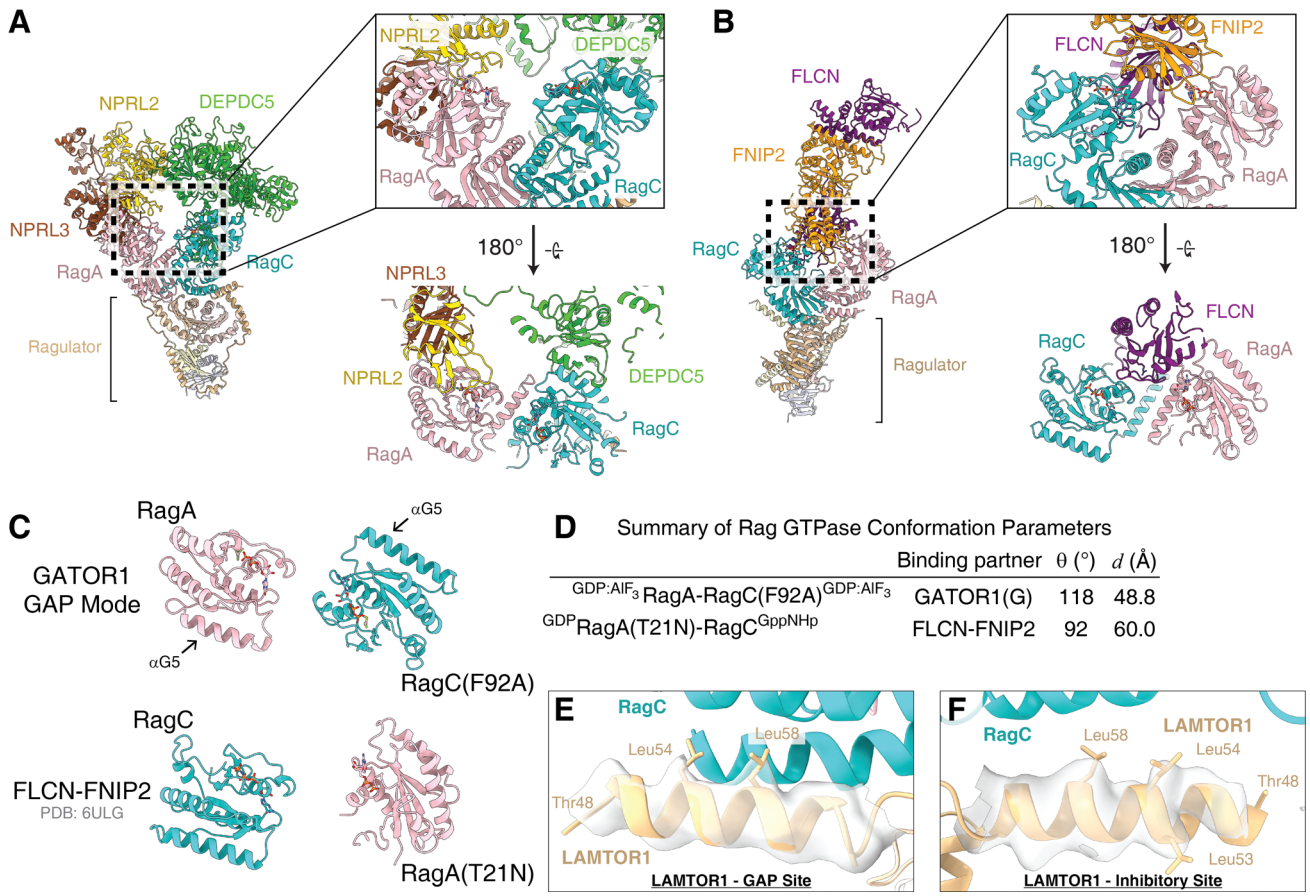

Figure S7. Impact of GATOR1 and FLCN-FNIP2 binding on Rag GTPase structure and conformation (Related to Figure 7).

A. Global (left) and local (right) architecture of the GATOR1-Rag-Ragulator complex in the GAP mode.
B. Global (left) and local (right) architecture of the FLCN-FNIP2-Rag-Ragulator complex.
C. Comparison of Rag GTPase conformation while bound to GATOR1 and FLCN-FNIP2. *d* measures the distance between the N-terminal tips of the two αG5 helices on the Rag GTPases. θ measures the angle formed by three points: the C- and N-terminal tips of the αG5 helix of RagA, and the N-terminal tip of the αG5 helix of RagC, thus reflecting the relative rotation.
D. Summary of Rag GTPase conformation parameters, θ and *d*, while bound to its upstream regulators.
E. N-terminal alpha helix of LAMTOR1 located at the GAP site in the dual mode GATOR1-Rag-Ragulator cryo-EM density map.
F. N-terminal alpha helix of LAMTOR1 located at the Inhibitory site in the dual mode GATOR1-Rag-Ragulator cryo-EM density map.